Clim. Past Discuss., 9, 2859–2887, 2013
www.clim-past-discuss.net/9/2859/2013/
doi:10.5194/cpd-9-2859-2013

Climate of the Past Discussions
Open Access

Using ice-flow models to evaluate potential sites of million year-old ice in Antarctica

B. Van Liefferinge and F. Pattyn

Laboratoire de Glaciologie, Université Libre de Bruxelles, CP 160/03,
Avenue F. D. Roosevelt 50, 1050 Brussels, Belgium

Received: 30 April 2013 – Accepted: 7 May 2013 – Published: 28 May 2013

Correspondence to: B. Van Liefferinge (bvlieffe@ulb.ac.be)

Published by Copernicus Publications on behalf of the European Geosciences Union.

Abstract

Finding suitable potential sites for an undisturbed record of million-year old ice in Antarctica requires a slow-moving ice sheet (preferably an ice divide) and basal conditions that are not disturbed by large topographic variations. Furthermore, ice should be thick and cold basal conditions should prevail, since basal melting would destroy the bottom layers. However, thick ice (needed to resolve the signal at sufficient high resolution) increases basal temperatures, which is a conflicting condition in view of finding a suitable drill site. In addition, slow moving areas in the center of ice sheets are also low-accumulation areas, and low accumulation reduces potential cooling of the ice through vertical advection. While boundary conditions such as ice thickness and accumulation rates are relatively well constraint, the major uncertainty in determining basal conditions resides in the geothermal heat flow (GHF) underneath the ice sheet. We explore uncertainties in existing GHF datasets and their effect on basal temperatures of the Antarctic ice sheet and propose an updated method based on Pattyn (2010) to improve existing GHF datasets in agreement with known basal temperatures and their gradients to reduce this uncertainty. Both complementary methods lead to a better comprehension of basal temperature sensitivity and a characterization of potential ice coring sites within these uncertainties.

1 Introduction

One of the major future challenges in the ice coring community is the search for a continuous and undisturbed ice core record dating back to 1.5 million years BP (Jouzel and Masson-Delmotte, 2010). The reason for such quest is that the oldest part of the EPICA Dome C ice core has revealed low values of CO_2 from 650 000 to 800 000 yr ago (Lüthi et al., 2008), which questions the strong Antarctic temperature-carbon cycle coupling on long time scales. Marine records show evidence of a reorganisation of the pattern of climate variability around 1 Myr ago, shifting from the "obliquity" dominated

CPD
9, 2859–2887, 2013

signal, characterized by 40 000 yr weak glacial-interglacial cycles to the "eccentricity"-dominated signal with longer glacial-interglacial cycles (Lisiecki and Raymo, 2005). The origin of this major climate reorganization (the so-called Mid-Pleistocene Transition, MPT) remains unknown and may be intrinsic to a series of feedback mechanisms between climate, cryosphere and carbon cycle (Jouzel and Masson-Delmotte, 2010). Alternatively, a recent study has demonstrated that climate oscillations over the past four million years can be explained by a single mechanism, i.e. the synchronization of nonlinear internal climate oscillations and the 413 000 yr eccentricity cycle (Rial et al., 2013). According to model calculations in conjunction with spectral analyisis, Rial et al. (2013) find that the climate system first synchronized to this 413 000 yr eccentricity cycle about 1.2 million years ago, roughly coinciding with this MPT.

Deep ice core drillings have been carried out in the past in Antarctica, reaching back in time over several hundred thousands of years. Amongst the longest records are Vostok (Petit et al., 1999), EPICA Dome Concordia (EPICA community members, 2004), Dome Fuji (Watanabe et al., 2003), and EPICA Dronning Maud Land (EPICA community members, 2006). The longest record is EPICA Dome Concordia, going back for more than 800 000 yr. Those records have in common that they are all recovered in the center of the ice sheet, and given the fact that the Antarctic ice sheet has been relatively constant in size ~~and~~ over the last 13 million years (DeConto and Pollard, 2003), they are consequently undisturbed by dramatic changes in ice flow, contrary to the longest records from the Greenland ice sheet (Johnson, 2001; NEEM community members, 2013).

In theory, and in absence of basal melting, these deep Antarctic records could reach several million years back in time with layers getting infinitesimally thin near the bottom. In reality, however, all deep records lack the bottom sequence as they are all found to be at pressure melting point and lower layers are melted away or heavily disturbed due to complex basal processes. Furthermore, resolving deep records not only requires that the bottom sequence is unaltered, but that the ice is sufficiently thick so that the gas

CPD
9, 2859–2887, 2013

signal can still be retrieved and analyzed with sufficient high resolution in the bottom layers.

In this paper we use several thermodynamic models to infer suitable areas for retrieving long ice-core records. We first investigate the most influential parameters having an effect on ice-core record length. Secondly, we apply this simple concept to evaluate uncertainties in GHF and use this uncertainty to guide the search for a suitable drilling place. Thirdly, we carry out a sensitivity analysis with a three-dimensional thermodynamical model (Pattyn, 2010) to determine the sensitivity of basal conditions to uncertainties in GHF, guided by a priori knowledge of basal conditions through the geographical distribution of subglacial lakes. ~~Results are discussed in the last section.~~

2 Why obvious drill sites are unsuitable

Obvious places to look for oldest ice are the deepest parts of the ice sheet, where ice is thick, and accumulation rates are low. However, a thick ice cover insulates very well and keeps the geothermal heat from escaping to the surface. Furthermore, we know that at least 379 subglacial lakes exist under the Antarctic ice sheet, which implies that large portions of the bedrock should be at pressure melting point (Smith et al., 2009; Pattyn, 2010; Wright and Siegert, 2012). Most subglacial lakes occur in the so-called Lakes District (stretching between Subglacial Lake Vostok and Wilkes Land in East Antarctica), characterized by a thick ice cover and also low geothermal heat flow (Shapiro and Ritzwoller, 2004; Pollard et al., 2005). Therefore, GHF is not the main culprit in causing subglacial melt.

The interplay between GHF and accumulation rates is very subtle, as high GHF increases basal temperatures, while high accumulation rates cool down the ice mass. To illustrate this we calculate the minimum GHF needed to reach pressure melting point at the bottom of any ice mass as a function of environmental parameters. This can easily be determined analytically (Hindmarsh, 1999; Siegert, 2000). Using the simplified

CPD
9, 2859–2887, 2013

model of Hindmarsh (1999), valid in the absence of horizontal ice advection due to motion, the minimum heat flow G_{min} needed to reach pressure melting point is

$$G_{\mathrm{min}} = \frac{k\,(T_0 - \gamma H - T_{\mathrm{s}})}{H(W(1) - W(0))}, \tag{1}$$

where

$$W(\zeta) = \int_1^{\zeta} \exp\left(\frac{\lambda(\zeta')H\dot{a}\rho c_p}{k}\right) \mathrm{d}\zeta', \tag{2}$$

and where

$$\lambda(\zeta) = \frac{\zeta^{n+3} - 1}{(n+1)(n+3)} - \frac{(n+2)(\zeta^2 - 1)}{2(n+1)} + \zeta - 1. \tag{3}$$

In Eqs. (1)–(3), H is the ice thickness, $T_0 = 273.15\,\mathrm{K}$ is the absolute temperature, T_{s} is the surface temperature (K), $k = 6.627 \times 10^7\,\mathrm{J\,m^{-1}\,yr^{-1}}$ is the thermal conductivity, $\rho = 910\,\mathrm{kg\,m^{-3}}$ is the ice density, $c_p = 2009\,\mathrm{J\,kg^{-1}\,K^{-1}}$ is the heat capacity, $\gamma = 8.7 \times 10^{-4}\,\mathrm{K\,m^{-1}}$ is derived from the Clausius–Clapeyron constant, $\dot{a}$ is the accumulation rate ($\mathrm{m\,yr^{-1}}$ IE, where IE stands for ice equivalent), and $n = 3$ is the exponent in Glen's flow law. Calculations are performed in a scaled coordinate system $\zeta \in [0, 1]$, where $\zeta = 0$ denotes the surface of the ice sheet. Equation (2) is solved using the quadrature method given in Hindmarsh (1999).

The result is illustrated in Fig. 1, displaying the minimum GHF needed to reach pressure melting point at the base of an ice sheet as a function of ice thickness H and surface accumulation rate $\dot{a}$, based on Eqs. (1)–(3) for a mean surface temperature $T_{\mathrm{s}} = -50\,^{\circ}\mathrm{C}$. Despite these low surface temperatures, pressure melting point is reached for relatively low values of GHF, as long as the ice is thick and accumulation rates are small, which is rather typical for the interior parts of the East Antarctic ice sheet. For

CPD
9, 2859–2887, 2013

high accumulation rates, one needs a significantly higher GHF to reach melting point at the base for a given ice thickness.

Even the low GHF values in Fig. 1 in conjunction with low accumulation rates are quite common over the central part of the East Antarctic ice sheet, which hampers the retrieval of a long time sequence under thick ice conditions. Despite the simplicity of the model, it can be applied to central parts of the Antarctic ice sheet (absence of horizontal advection) to explore suitable drill sites as a function of known (or estimated) geothermal heat fluxes.

3 Uncertainties in Antarctic GHF and the oldest ice

3.1 Data sets and model setup

The above simple model is applied to central areas of the Antarctic ice sheet that are characterized by slow ice motion, hence the vicinity of ice divides. To do so, ice thickness is taken from the recent BEDMAP2 compilation (Fretwell et al., 2013) and resampled on a 5 km grid. Surface mass balance is obtained from van de Berg et al. (2006) and van den Broeke et al. (2006), based on the output of a regional atmospheric climate model for the period 1980 to 2004 and calibrated using observed mass balance rates. Surface temperatures are due to van den Broeke (2008), based on a combined regional climate model, calibrated with observed 10 m ice temperatures. Using these datasets enables us to calculate the minimum required GHF to reach pressure melting point at the bed. Since the model is along the vertical dimension, it is only valid for divide areas. The simulations are therefore only carried out for horizontal velocities smaller than 2 m yr^{-1}. Ice sheet velocities in divide areas are determined based on balance velocities, stating that the mass of ice flowing out of any area within the horizontal domain (x, y) exactly equals the sum of the inflow and the ice accumulated over the area (Budd and Warner, 1996; Fricker et al., 2000; Le Brocq et al., 2006),

$$\nabla_{\mathrm{H}} \boldsymbol{q}_{\mathrm{s}} = \dot{a}, \tag{4}$$

CPD
9, 2859–2887, 2013

with

$$\boldsymbol{q}_{\mathrm{s}} = -H \int_{b}^{s} \boldsymbol{v}_{\mathrm{H}}(z')\mathrm{d}z', \tag{5}$$

and where b and s are the bottom and the surface of the ice sheet (m a.s.l.), respectively. Integrating Eq. (4) over the whole surface of the ice sheet, starting at the ice divides, one obtains the vertically averaged horizontal balance velocities $\overline{\boldsymbol{v}}_{\mathrm{H}} = (\overline{v}_x, \overline{v}_y)$. Details of this procedure are given in Pattyn (2010).

Using the above datasets, the minimum geothermal heat flow G_{min} from Eq. (1) needed to reach pressure melting point at the bed is calculated for the areas of the Antarctic ice sheet where horizontal flow velocities are $< 2\,\mathrm{m\,yr^{-1}}$ and where ice thickness $H > 2000\,\mathrm{m}$. This ice thickness is considered to be the lower limit for possibly recovery of a million-year old climate signal (H. Fischer, personal communication, 2013). The calculated values of G_{min} are subsequently compared to known values of GHF.

Several datasets of derived GHF underneath the Antarctic ice sheet exist. The first one (G_1) uses a global seismic model of the crust and the upper mantle to guide the extrapolation of existing heat-flow measurements to regions where such measurements are rare or absent (Shapiro and Ritzwoller, 2004). The second GHF database (G_2) stems from satellite magnetic measurements (Fox-Maule et al., 2005). Values of GHF are in the same range as Shapiro and Ritzwoller (2004), but the spatial variability is contrasting. Heat flow measurements according to Fox-Maule et al. (2005) are also considerably higher than those by Shapiro and Ritzwoller (2004). A third dataset is due to Puruker (2013). This geothermal heat flux data set (G_3) is based on low resolution observations collected by the CHAMP satellite between 2000 and 2010, and produced from the MF-6 model following the technique described in Fox-Maule et al. (2005). While the technique is similar, GHF values are considerably lower than the latter, and even lower than those derived from the seismic model (Shapiro and Ritzwoller, 2004).

CPD
9, 2859–2887, 2013

3.2 Results

In view of the large uncertainty in GHF estimates, we combined all three datasets into two databases, i.e. a mean GHF, $\overline{G}$, and a standard deviation, σ_G. The latter is calculated based on the inter-database variability and the standard deviation given for the Shapiro and Ritzwoller (2004) dataset in the following way:

$$\sigma_G = \sigma\left[G_1 - \sigma(G_1), G_1 + \sigma(G_1), G_2, G_3\right]. \quad (6)$$

Both are depicted in Fig. 2. High values of σ_G indicate a large dispersion between the three datasets. These are essentially found in West Antarctica and along the Transantarctic Mountains. The lowest values are restricted to the central parts of the East-Antarctic continent.

The calculated values of $G_{\min}$ are directly compared to the map of mean GHF. For $G_{\min} < \overline{G}$, the observed GHF is too elevated to prevent the bottom ice to reach pressure melting and most likely (within error bounds) the ice is temperate. For $G_{\min} > \overline{G}$ the minimum GHF needed to reach pressure melting at the base is higher than the value reported. Of course, this information needs to be further evaluated against the dispersion between the GHF datasets, represented by σ_G. The result is shown in Fig. 3, where the rectangular area points to the potentially most suitable conditions in terms of basal temperature, i.e. the largest difference between actual GHF and minimum GHF in combination with the lowest variability between the three GHF datasets. The furthest to the right in Fig. 3, the colder the bed because a significant higher GHF than observed is needed to make the bed temperate; the lower the value of σ_G, the more likely there is a small spread (hence reduced uncertainty) in GHF, so that the observed value is likely. On top of this, the color scale shows the ice thickness for each of the points. The thickest ice is obviously corresponding to zones that are temperate (negative values of ΔG), while for large positive ΔG and small σ_G, ice is also the thinnest.

These restrictions (superposed on the ice flow speed limit and minimum ice thickness) lead to a few areas in the central part of the Antarctic ice sheet that are

CPD
9, 2859–2887, 2013

considered suitable for cold-bed conditions. The largest zone is situated near Dome Argus on top of the Gamburtsev subglacial Mountains (Fig. 4). However, subglacial mountain ranges are likely characterized by an accidented bed topography (Bell et al., 2011), which may also hamper the interpretation of the paleo-climatic signal (Grootes et al., 1993). Other potential areas are situated around Dome Fuji as well as on Ridge B, between Subglacial Lake Vostok and Dome Argus. The Dome Concordia area seems less prone to cold basal conditions, due to the large uncertainty in GHF and the thick ice, which makes temperate conditions more acceptable.

4 Thermomechanical ice-flow modelling

The simple thermodynamic model used in the previous section neglects horizontal advection, which – even in the interior of the Antarctic ice sheet – will play a significant role in changing the thermal properties of the ice/bed interface. In the next section we present a more advanced thermomechical ice-sheet model to calculate basal temperatures for a set of given boundary conditions and applied to the whole Antarctic ice sheet. Moreover, we try to reduce uncertainties in GHF by incorporating actual information on bed properties, such as the geographical distiribution of subglacial lakes.

4.1 Model description

The thermodynamical model used for this purpose is the same as described in detail in Pattyn (2010). The major differences are related to the way the horizontal flow field is calculated. Moreover, we use a new series of datasets on ice thickness (see Sect. 3.1) and geothermal heat flow.

The thermodynamic equation for the temperature distribution in an ice mass is given by

$$\rho c_p \frac{\partial T}{\partial t} = \nabla(k\nabla T) - \rho c_p \boldsymbol{v} \cdot \nabla T - 2\dot{\varepsilon}\sigma, \quad (7)$$

CPD
9, 2859–2887, 2013

where T is the ice temperature (K) and $\boldsymbol{v} = (v_x, v_y, v_z)$ is the three-dimensional ice velocity vector ($\mathrm{m\,yr^{-1}}$). The last term on the right-hand side represents internal heating rate per unit volume (Pattyn, 2003), where $\dot{\varepsilon}$ and σ are effective strain rate and effective shear stress, respectively. Horizontal diffusion is neglected, and the temperature field is considered to be in steady state ($\frac{\partial T}{\partial t} = 0$).

Boundary conditions for Eq. (7) are the surface temperature T_s and a basal temperature gradient, based on the geothermal heat flux:

$$\left.\frac{\partial T}{\partial z}\right|_b = -\frac{1}{k}(G + \tau_b \boldsymbol{v}_b), \tag{8}$$

where G is the geothermal heat flux entering the base of the ice sheet and the second term on the right-hand side of (8) heat produced due to basal sliding. τ_b is the basal shear stress, and can be defined as $\tau_b = -\rho g H \nabla_H s$, where $\nabla_H s$ is the surface slope. Whenever pressure melting point is reached, the temperature in the ice is kept at this value $T_{pmp} = T_0 - \gamma(s - z)$.

4.2 Velocity field

Ice sheet velocities are obtained from a combination of observed velocities from satellite radar interferometry and modelled velocities. Satellite-derived velocities are available for almost the entire continent (Rignot et al., 2011), but are only relevant in the coastal areas and for fast ice flow. Generally spoken, the error associated with the slow flowing areas is substantially higher than 100 %. Furthermore, in vicinity of the South Pole, interferometric velocities are lacking due to the sun-synchronous orbit of satellites. To fill in the gaps and to guarantee a continuous flow field for our simulations, a heuristic method was implemented that uses interferometrically-derived velocities for flow speeds above $100\,\mathrm{m\,yr^{-1}}$ and modelled velocities for flow speeds below $15\,\mathrm{m\,yr^{-1}}$. Modelled velocities are derived from balance velocities, described in Sect. 3. Between 15 and $100\,\mathrm{m\,yr^{-1}}$, both modelled and interferometric velocities are combined as a

CPD
9, 2859–2887, 2013

fraction of flow speed, in order to keep the transition between both datasets as smooth as possible and to guarantee a correct flow direction.

The three-dimensional horizontal velocities are then determined from the shallow-ice approximation (Hutter, 1983), by

$$\boldsymbol{v}_{\mathrm{H}}(x,y,\zeta) = \left(\frac{n+2}{n+1}\overline{\boldsymbol{v}}_{\mathrm{H}} - \boldsymbol{v}_{\mathrm{b}}\right)\left(1-\zeta^{n+1}\right) + \boldsymbol{v}_{\mathrm{b}}\,, \tag{9}$$

where basal sliding $\boldsymbol{v}_{\mathrm{b}}$ is represented by a Weertman sliding law (Pattyn, 2010). The vertical velocity field is derived from mass conservation combined with the incompressibility condition for ice. Given an ice sheet in steady state, a simple analytical expression can be obtained, based on the horizontal balance velocities (Hindmarsh, 1999; Hindmarsh et al., 2009). Expressed in local coordinates, and in the absence of subglacial melting, this leads to

$$v_{\zeta}(x,y,\zeta) = -\left[\frac{\zeta^{n+2} - 1 + (n+2)(1-\zeta)}{n+1}\right]\dot{a} + \boldsymbol{v}_{\mathrm{H}}\nabla b + (1-\zeta)\boldsymbol{v}_{\mathrm{H}}\nabla H. \tag{10}$$

The numerical solution of the model is detailed in Pattyn (2010). For all experiments, $n = 3$ was used, which corresponds to the isothermal case. However, in the thermomechanically-coupled case, the exponent is larger (Ritz, 1987), which results in a different shape of the vertical velocity profile, hence advection being more concentrated to the surface, leading to warmer basal conditions compared to the isothermal case. However, this effect is most pronounced in areas where horizontal velocity gradients $\partial v_x/\partial x$, $\partial v_y/\partial y$ are more important. Since we concentrate on the central areas of the ice sheet, this bias (underestimation of basal temperatures) will have a limited effect.

CPD
9, 2859–2887, 2013

4.3 Input data calibration

Major input datasets are already described in Sect. 3. In this section, we will focus on the improvements made to the initial GHF datasets in order to reduce uncertainty on GHF.

Direct measurements of GHF are very rare, and are usually obtained from temperature measurements in boreholes of deep ice core drillings. Basal temperature gradients in observed temperature profiles of deep boreholes, compared with values from the three GHF datasets, show rather large discrepancies. Therefore, the three GHF datasets were corrected using observed basal temperature gradients, surface temperature and accumulation rates, in such a way that modeled temperature profiles match as close as possible the observed ones (Pattyn, 2010).

This type of correction is made for sites where temperature profiles are available, i.e. Byrd (Gow et al., 1968), Taylor Dome (G. Clow and E. Waddington, personal communication, 2008), Siple Dome (MacGregor et al., 2007), Law Dome (Dahl-Jensen et al., 1999; van Ommen et al., 1999), Vostok (Salamatin et al., 1994; Parrenin et al., 2004), South Pole (Price et al., 2002), Dome Fuji (Fujii et al., 2002; Hondoh et al., 2002), EPICA Dome C (Parrenin et al., 2007, C. Ritz, personal communication, 2008), and EPICA DML (Ruth et al., 2007). The applied method consists of determining the difference between observed (o) and corresponding database values and to adapt a Gaussian function for a sufficient large influence area. For a variable in the database X (either surface accumulation, surface temperature or geothermal heat flux), its corrected value X_c based on an observation X_o is obtained by

$$X_c(x,y) = X + [X_o - X] \exp\left[-\frac{x^2+y^2}{\sigma^2}\right], \quad (11)$$

where (x,y) is the horizontal distance from this observed position (0,0). The influence area is dictated by σ and calculations were performed for $\sigma = 0$, 20, 50, 100, and 200 km (a discussion on the choice of these values is given below). As such, by

CPD
9, 2859–2887, 2013

tuning GHF (constraining the vertical temperature gradient) and surface mass balance (constraining vertical advection), the difference between modeled and observed temperature profiles is less than 2 K. The remaining difference is still due to horizontal advection, which is a model output, as well as past changes in surface temperature that were not taken into account in the model.

4.4 Subglacial lake correction

Numerous subglacial lakes have been identified from radio-echo sounding. An initial inventory brought their number on 145 (Siegert et al., 2005), and more than 230 have been added since (Bell et al., 2006, 2007; Carter et al., 2007; Popov and Masolov, 2007; Fricker et al., 2007; Fricker and Scambos, 2009; Smith et al., 2009), leading to a total number of 379 lakes of varying size (Wright and Siegert, 2012). Subglacial lakes are usually identified from radio-echo sounding (RES) and characterized by a strong basal reflector and a constant echo strength (corroborating a smooth surface) or identified through surface elevation changes using satellite altimetry, corroborating sudden subglacial water discharge (Fricker et al., 2007; Pattyn, 2011).

Subglacial lakes are used to constrain the GHF datasets, considering them to be at pressure melting point. As such, we calculate the minimum GHF needed to reach pressure melting point using Eq. (1) for any position of a subglacial lake. The value for G_{min} thus obtained is a minimum value, which means that if at that spot the database contains a higher value, the latter is retained. Spatial corrections are subsequently applied using the Gaussian function defined in Eq. (11) for different influence areas as defined above.

5 Ensemble model results

The temperature field in the ice sheet was calculated for 15 different sets of boundary conditions, i.e. the three datasets of GHF (Shapiro and Ritzwoller, 2004; Fox-Maule

CPD
9, 2859–2887, 2013

et al., 2005; Puruker, 2013), and each of the datasets corrected for subglacial lakes and existing temperature profiles for influence area size $\sigma = 0$ (no correction), 20, 50, 100, and 200 km, respectively. The result is given in Fig. 5, representing the mean basal temperature of the 15 experiments, corrected for the dependence on pressure melting, and the RMSE (Root Mean Square Error) corresponding to the different experiments.

Low values of RMSE correspond to zones where correction is effective and the difference between the experiments is low, or areas that despite the variability in GHF are always at pressure melting point. This is the case for the central part of the West-Antarctic ice sheet, as well as extensive zones in the Lakes District, where the dense network of subglacial lakes keeps the bed at melting point.

Based on the ensemble experiments, the relation between accumulation (vertical advection), ice thickness and basal temperature is less straightforward than with the simple model. The focus of the full model is to reduce uncertainties on GHF using proxy data, and therefore the RMSE guides us towards more suitable sites. Figure 6 summarizes the most suitable drilling areas based on the full model for flow speeds lower than $2\,\mathrm{m\,yr^{-1}}$, ice thickness $H > 2000\,\mathrm{m}$, and a basal temperature lower than $-5\,^{\circ}\mathrm{C}$. The color scale denotes the RMSE based on the ensemble experiments. We deliberately excluded basal temperatures higher than $-5\,^{\circ}\mathrm{C}$, a value considered to be sufficiently away from the melting point in view of our model approximations. Suitable areas characterized by low values of RMSE (hence smaller spread in basal temperatures according to the ensemble experiments) are found near existing ice core sites where a temperature gradient is at hand, i.e. Dome Concordia, Dome Fuji and Vostok. Since all three sites are at or close to pressure melting point at the base, suitable cold-based sites are not exactly situated at those spots, but in their vicinity where ice is slightly thinner.

Similar to the simple model, suitable sites (sufficiently low basal temperature) are found in the Gamburtsev Mountain region as well as along Ridge B. However, the ensemble analysis results in a larger spread of basal temperature range due to either the lack of basal temperature gradient constraints and/or the absence of subglacial

CPD
9, 2859–2887, 2013

lakes. Both regions are characterized by relatively low basal temperatures (Fig. 5) and are unlikely to reach pressure melting point, despite the large RMSE due to – mainly – differences between the GHF datasets.

6 Discussion and conclusions

Since both the simple and ensemble model results are complementary (but not totally independent) in nature, they can be combined to form a joint dataset. The analysis is limited to flow speeds lower than 2 m yr^{-1} and ice thickness $H > 2000$ m, which are considered as suitable conditions for retrieving and resolving ice older than one million years. Given the uncertainty in GHF originating from the large dispersion between the different datasets (both spatially and in terms of absolute values), we put constraints on the selection of suitable sites: (i) the minimum GHF needed to reach pressure melting point should at least be 5 mW m^{-2} higher than the mean value from the combined GHF datasets; (ii) the variability between the GHF datasets for a given site expressed by the standard deviation σ_G should equally be less than 25 mW m^{-2}; (iii) the mean basal temperature according to the ensemble model calculations should be less than −5 °C (but lower values are favored). Results are displayed in Fig. 7. We explored different values for these constraints, but the general pattern remains the same. The main effect is the stronger the constraint, the smaller the areas, but the geographical distribution is not altered.

Due to the velocity and ice thickness constraints, all sites are situated near the ice divides. Not surprisingly, areas near the major drill sites and where temperature profiles are available (Dome Fuji, Dome Concordia, Vostok and South Pole), are also retained. These are not the sites themselves, but zones of smaller ice thickness in their vicinity. Finally, suitable areas are found across the Gamburtsev Mountains and Ridge B (between Dome Argus and Vostok). The former is characterized by a much larger spatial variability in bedrock topography, while the latter may suffer from a lack in decent constraints on ice thickness (according to Fig. 2 in Fretwell et al., 2013).

CPD
9, 2859–2887, 2013

Subglacial topography is a key factor in determining suitable sites for oldest ice. Given the strong relationship between basal temperatures and ice thickness, as depicted by Fig. 1, it is quite likely to find suitable cold-based spots in the vicinity of deep ice core sites that have the bottom ice at or near pressure melting point. Areas that should be avoided are those in which a large number of subglacial lakes are found, such as the Lakes District, where even low values of GHF are sufficient to keep the ice at pressure melting.

Another factor that may influence basal conditions is due to the glacial-interglacial history of the ice sheet and the time-scales needed for the ice sheet to thermally adapt to different climates. Moreover, the temperature calculations made in this study are based on present-day observed parameters of surface temperature, ice thickness and accumulation rate. To test this effect, we calculated the minimum geothermal heat flow G_{min} needed to keep the base at pressure melting point for environmental conditions that are the mean for a longer time span. We reduced the surface temperature T_{s} by 6 K, reduced the surface accumulation rate $\dot{a}$ to 60 % of its current value, and reduced ice thickness H with 100 m, which is valid for the divide areas. The results are surprisingly coherent with the previously-calculated values, and are therefore not shown separately. The main reason is that for this spread of values the reduced accumulation rate (which reduces vertical advection, hence warms the bottom ice layers) is largely counteracted by the decrease in surface temperature. However, one needs to keep in mind that both calculations (present-day and mean glacial-interglacial) relate to steady-state conditions, which in reality is not the case.

Nevertheless, one should be careful in using the above model results as a sole guide in the process of detecting suitable cold-based areas for retrieving a long ice-core record, due to a number of factors that were not taken into account:

1. Areas characterized by subglacial mountains or other bedrock variability may well be suitable from a thermal point of view, the topographic variability may well hamper the deciphering of the climate signal due to complex processes, such as ice overturning (NEEM community members, 2013) or refreezing (Bell et al., 2011).

CPD
9, 2859–2887, 2013

2. The upper limit on the flow velocity of $2\,\mathrm{m\,yr^{-1}}$ may also be too high for reconstructing the climate signal without having to rely to heavily on ice flow models for correcting for upstream advection. In theory, ice could have traveled over several hundreds of kilometers before reaching the ice core site, and this without taking into account any shifts in ice divides over glacial-interglacial periods, which would also influence the flow direction over time.

3. The spatial variability of GHF may in realty be much higher than the one represented in the three GHF datasets.

4. Areas where bedrock data is unavailable (or where interpolation is based on sparse data) may be wrongly classified in the above analysis, and some suitable areas thus overseen.

While this paper gives an overview of continental-scale basal conditions of the Antarctic ice sheet, the processed datasets from both the simple ($\overline{G}$, σ_G) and the full model ($\overline{T}$, RMSE_T) will be made available online together with simple MatLab scripts to allow for a more detailed search/zoom for potential sites, based on the figures presented here.

Acknowledgements. This paper forms a contribution to the FNRS–FRFC project (Fonds de la Recherche Scientifique) entitled “NEEM: The Eemian and beyond in Greenland ice”. The authors are indebted to C. Ritz for valuable discussions and commenting on an earlier version of the manuscript.

CPD
9, 2859–2887, 2013

References

Bell, R. E., Studinger, M., Fahnestock, M. A., and Shuman, C. A.: Tectonically controlled subglacial lakes on the flanks of the Gamburtsev Subglacial Mountains, East Antarctica, Geophys. Res. Letters, 33, L02504, doi:10.1029/2005GL025207, 2006. 2871

Bell, R. E., Studinger, M., Fahnestock, C. A. S. M. A., and Joughin, I.: Large subglacial lakes in East Antarctica at the onset of fast-flowing ice streams, Nature, 445, 904–907, doi:10.1038/nature05554, 2007. 2871

Bell, R. E., Ferraccioli, F., Creyts, T. T., Braaten, D., Corr, H., Das, I., Damaske, D., Frearson, N., Jordan, T., Rose, K., Studinger, M., and Wolovick, M.: Widespread persistent thickening of the East Antarctic ice sheet by freezing from the base, Science, 331, 1592–1595, 2011. 2867, 2874

Budd, W. F. and Warner, R. C.: A computer scheme for rapid calculations of balance–flux distributions, Ann. Glaciol., 23, 21–27, 1996. 2864

Carter, S. P., Blankenship, D. D., Peters, M. F., Young, D. A., Holt, J. W., and Morse, D. L.: Radar-based subglacial lake classification in Antarctica, Geochem. Geophy. Geosy., 8, Q03016, doi:10.1029/2006GC001408, 2007. 2871

Dahl-Jensen, D., Morgan, V. I., and Elcheikh, A.: Monte Carlo inverse modelling of the Law Dome (Antarctica) temperature profile, Ann. Glaciol., 29, 145–150, 1999. 2870

DeConto, R. M. and Pollard, D.: Rapid Cenozoic glaciation of Antarctica induced by declining atmospheric CO_2, Nature, 421, 245–249, 2003. 2861

EPICA community members: Eight glacial cycles from an Antarctic ice core, Nature, 429, 623–628, 2004. 2861

EPICA community members: One-to-one coupling of glacial climate variability in Greenland and Antarctica, Nature, 444, 195–198, 2006. 2861

Fox-Maule, C., Purucker, M. E., Olsen, N., and Mosegaard, K.: Heat flux anomalies in Antarctica revealed by satellite magnetic data, Science, 309, 464–467, 2005. 2865, 2871, 2882

Fretwell, P., Pritchard, H. D., Vaughan, D. G., Bamber, J. L., Barrand, N. E., Bell, R., Bianchi, C., Bingham, R. G., Blankenship, D. D., Casassa, G., Catania, G., Callens, D., Conway, H., Cook, A. J., Corr, H. F. J., Damaske, D., Damm, V., Ferraccioli, F., Forsberg, R., Fujita, S., Gim, Y., Gogineni, P., Griggs, J. A., Hindmarsh, R. C. A., Holmlund, P., Holt, J. W., Jacobel, R. W., Jenkins, A., Jokat, W., Jordan, T., King, E. C., Kohler, J., Krabill, W., Riger-Kusk, M., Langley, K. A., Leitchenkov, G., Leuschen, C., Luyendyk, B. P., Matsuoka, K.,

CPD
9, 2859–2887, 2013

Mouginot, J., Nitsche, F. O., Nogi, Y., Nost, O. A., Popov, S. V., Rignot, E., Rippin, D. M., Rivera, A., Roberts, J., Ross, N., Siegert, M. J., Smith, A. M., Steinhage, D., Studinger, M., Sun, B., Tinto, B. K., Welch, B. C., Wilson, D., Young, D. A., Xiangbin, C., and Zirizzotti, A.: Bedmap2: improved ice bed, surface and thickness datasets for Antarctica, The Cryosphere, 7, 375–393, doi:10.5194/tc-7-375-2013, 2013. 2864, 2873

Fricker, H. A. and Scambos, T.: Connected subglacial lake activity on lower Mercer and Whillans Ice Streams, West Antarctica, 2003–2008, J. Glaciol., 55, 303–315, 2009. 2871

Fricker, H. A., Warner, R., and Allison, I.: Mass balance of the Lambert Glacier-Amery Ice Shelf system, East Antarctica: a comparison of computed balance fluxes and measured fluxes, J. Glaciol., 46, 561–570, 2000. 2864

Fricker, H. A., Scambos, T., Bindschadler, R., and Padman, L.: An active subglacial water system in West Antarctica mapped from space, Science, 315, 1544–1548, doi:10.1126/science.1136897, 2007. 2871

Fujii, Y., Azuma, N., Tanaka, Y., Nakayama, M., Kameda, T., Shinbori, K., Katagiri, K., Fujita, S., Takahashi, A., Kawada, K., Motoyama, H., Narita, H., Kamiyama, K., Furukawa, T., Takahashi, S., Shoji, H., Enomoto, H., Sitoh, T., Miyahara, T., Naruse, R., Hondoh, T., Shiraiwa, T., Yokoyama, K., Ageta, Y., Saito, T., and Watanabe, O.: Deep ice core drilling to 2503 m depth at Dome Fuji, Antarctica, Mem. Natl Inst. Polar Res., Spec. Issue, 56, 103–116, 2002. 2870

Gow, A. J., Ueda, H. T., and Garfield, D. E.: Antarctic ice sheet – preliminary results of first core hole to bedrock, Science, 161, 1011–1013, 1968. 2870

Grootes, P. M., Stuiver, M., White, J. W. C., Johnson, S., and Jouzel, J.: Comparison of oxygen isotope records from the GISP2 and GRIP Greenland ice cores, Nature, 366, 552–554, 1993. 2867

Hindmarsh, R. C. A.: On the numerical computation of temperature in an ice sheet, J. Glaciol., 45, 568–574, 1999. 2862, 2863, 2869

Hindmarsh, R. C. A., Leysinger Vieli, G. J. M. C., and Parrenin, F.: A large-scale numercial model for computing isochrone geometry, Ann. Glaciol., 50, 130–140, 2009. 2869

Hondoh, T., Shoji, H., Watanabe, O., Salamatin, A. N., and Lipenkov, V.: Depth-age and temperature prediction at Dome Fuji Station, East Antarctica, Ann. Glaciol., 35, 384–390, 2002. 2870

Hutter, K.: Theoretical Glaciology, Kluwer Academic Publishers, Dordrecht, 1983. 2869

CPD
9, 2859–2887, 2013

Johnson, S.: Oxygen isotope and palaeotemperature records from six Greenland ice-core stations: Camp Century, Dye-3, GRIP, GISP2, Renland and NorthGRIP, J. Quaternary Sci., 16, 299–307, 2001. 2861

Jouzel, J. and Masson-Delmotte, V.: Deep ice cores: the need for going back in time, Quaternary Sci. Rev., 29, 3683–3689, 2010. 2860, 2861

Le Brocq, A. M., Payne, A. J., and Siegert, M. J.: West Antarctic balance calculations: impact of flux-routing algorithm, smoothing algorithm and topography, Comput. Geosci., 32, 1780–1795, 2006. 2864

Lisiecki, L. E. and Raymo, M. E.: A Pliocene-Pleistocene stack of 57 globally distributed benthic δ^{18}O records, Paleoceanography, 20, PA1003, doi:10.1029/2004PA001071, 2005. 2861

Lüthi, D., Lefloch, M., Bereiter, B., Blunier, T., Barnola, J. M., Siegenthaler, U., Raynaud, D., Jouzel, J., Fischer, H., Kawamura, K., and Stocker, T. F.: High-resolution carbon dioxide concentration record 650 000–800 000 years before present, Nature, 453, 379–382, 2008. 2860

MacGregor, J. A., Winebrenner, D. P., Conway, H., Matsuoka, K., Mayewski, P. A., and Clow, G. D.: Modeling englacial radar attenuation at Siple Dome, West Antarctica, using ice chemistry and temperature data, J. Geophys. Res., 112, F03008, doi:10.1029/2006JF000717, 2007. 2870

NEEM community members: Eemian interglacial reconstructed from a Greenland folded ice core, Nature, 493, 489–494, 2013. 2861, 2874

Parrenin, F., Remy, F., Ritz, C., Siegert, M., and Jouzel, J.: New modelling of the Vostok ice flow line and implication for the glaciological chronology of the Vostok ice core, J. Geophys. Res., 109, D20102, doi:10.1029/2004JD004561, 2004. 2870

Parrenin, F., Dreyfus, G., Durand, G., Fujita, S., Gagliardini, O., Gillet, F., Jouzel, J., Kawamura, K., Lhomme, N., Masson-Delmotte, V., Ritz, C., Schwander, J., Shoji, H., Uemura, R., Watanabe, O., and Yoshida, N.: 1-D-ice flow modelling at EPICA Dome C and Dome Fuji, East Antarctica, Clim. Past, 3, 243–259, doi:10.5194/cp-3-243-2007, 2007. 2870

Pattyn, F.: A new 3-D higher-order thermomechanical ice-sheet model: basic sensitivity, ice-stream development and ice flow across subglacial lakes, J. Geophys. Res., 108, 2382, doi:10.1029/2002JB002329, 2003. 2868

Pattyn, F.: Antarctic subglacial conditions inferred from a hybrid ice sheet/ice stream model, Earth Planet. Sc. Lett., 295, 451–461, 2010. 2860, 2862, 2865, 2867, 2869, 2870

CPD
9, 2859–2887, 2013

Pattyn, F.: Antarctic subglacial lake discharges, in: Antarctic Subglacial Aquatic Environments, edited by: Siegert, M. and Bindschadler, B., doi:10.1029/2010GM000935, AGU, Washington D.C., 2011. 2871

Petit, J. R., Jouzel, J., Raynaud, D., Barkov, N. I., Barnola, J. M., Basile, I., Bender, M., Chappellaz, J., Davis, M., Delaygue, G., Delmotte, M., Kotlyakov, V., Legrand, M., Lipenkov, V. Y., Lorius, C., Pepin, L., Ritz, C., Saltzman, E., and Stievenard, M.: Climate and atmospheric history of the past 420 000 years from the Vostok ice core, Antarctica, Nature, 399, 429–436, 1999. 2861

Pollard, D., DeConto, R. M., and Nyblade, A. A.: Sensitivity of Cenozoic Antarctic ice sheet variations to geothermal heat flux, Global Planet. Change, 49, 63–74, 2005. 2862

Popov, S. V. and Masolov, V. N.: Forty-seven new subglacial lakes in the 0–110° sector of East Antarctica, J. Glaciol., 53, 289–297, 2007. 2871

Price, P. B., Nagornov, O. V., Bay, R., Chirkin, D., He, Y., Miocinovic, P., Richards, A., Woschnagg, K., Koci, B., and Zagorodnov, V.: Temperature profile for glacial ice at the South Pole: implications for life in a nearby subglacial lake, P. Natl. Acad. Sci. USA, 99, 7844–7847, 2002. 2870

Puruker, M.: Geothermal heat flux data set based on low resolution observations collected by the CHAMP satellite between 2000 and 2010, and produced from the MF-6 model following the technique described in Fox Maule et al. (2005), available at: http://websrv.cs.umt.edu/isis/index.php, last access: 23 March 2013. 2865, 2872, 2882

Rial, J. A., Oh, J., and Reischmann, E.: Synchronization of the climate system to eccentricity forcing and the 100 000-year problem, Nat. Geosci., 6, 289–293, 2013. 2861

Rignot, E., Mouginot, J., and Scheuchl, B.: Ice flow of the antarctic ice sheet, Science, 333, 1427–1430, 2011. 2868

Ritz, C.: Time Dependent Boundary Conditions for Calculation of Temperature Fields in Ice Sheets, IAHS Publ., 170, 207–216, 1987. 2869

Ruth, U., Barnola, J.-M., Beer, J., Bigler, M., Blunier, T., Castellano, E., Fischer, H., Fundel, F., Huybrechts, P., Kaufmann, P., Kipfstuhl, S., Lambrecht, A., Morganti, A., Oerter, H., Parrenin, F., Rybak, O., Severi, M., Udisti, R., Wilhelms, F., and Wolff, E.: "EDML1": a chronology for the EPICA deep ice core from Dronning Maud Land, Antarctica, over the last 150 000 years, Clim. Past, 3, 475–484, doi:10.5194/cp-3-475-2007, 2007. 2870

CPD
9, 2859–2887, 2013

Salamatin, A. N., Lipenkov, V. Y., and Blinov, K. V.: Vostok (Antarctica) climate record time-scale deduced from the analysis of a borehole-temperature profile, Ann. Glaciol., 20, 207–214, 1994. 2870

Shapiro, N. M. and Ritzwoller, M. H.: Inferring surface heat flux distributions guided by a global seismic model: particular application to Antarctica, Earth Planet. Sc. Lett., 223, 213–224, 2004. 2862, 2865, 2866, 2871, 2882

Siegert, M. J.: Antarctic subglacial lakes, Earth-Sci. Rev., 50, 29–50, 2000. 2862

Siegert, M. J., Carter, S., Tobacco, I., Popov, S., and Blankenship, D.: A revised inventory of Antarctic subglacial lakes, Antarct. Sci., 17, 453–460, 2005. 2871

Smith, B. E., Fricker, H. A., Joughin, I. R., and Tulaczyk, S.: An inventory of active subglacial lakes in Antarctica detected by ICESat (2003–2008), J. Glaciol., 55, 573–595, 2009. 2862, 2871

van de Berg, W. J., van den Broeke, M. R., Reijmer, C. H., and van Meijgaard, E.: Reassessment of the Antarctic surface mass balance using calibrated output of a regional atmospheric climate model, J. Geophys. Res, 111, D11104, doi:10.1029/2005JD006495, 2006. 2864

van den Broeke, M. R.: Depth and density of the Antarctic firn layer, Arct. Antarct. Alp. Res., 40, 432–438, 2008. 2864

van den Broeke, M. R., van de Berg, W. J., and van Meijgaard, E.: Snowfall in coastal West Antarctica much greater than previously assumed, Geophys. Res. Lett., 33, L02505, doi:10.1029/2005GL025239, 2006. 2864

van Ommen, T. D., Morgan, V. I., Jacka, T. H., Woon, S., and Elcheikh, A.: Near-surface temperatures in the Dome Summit South (Law Dome, East Antarctica) borehole, Ann. Glaciol., 29, 141–144, 1999. 2870

Watanabe, O., Jouzel, J., Johnsen, S., Parrenin, F., Shoji, H., and Yoshida, N.: Homogeneous climate variability across East Antarctica over the past three glacial cycles, Nature, 422, 509–512, 2003. 2861

Wright, A. P. and Siegert, M. J.: A fourth inventory of Antarctic subglacial lakes, Antarct. Sci., 24, 659–664, 2012. 2862, 2871

CPD
9, 2859–2887, 2013

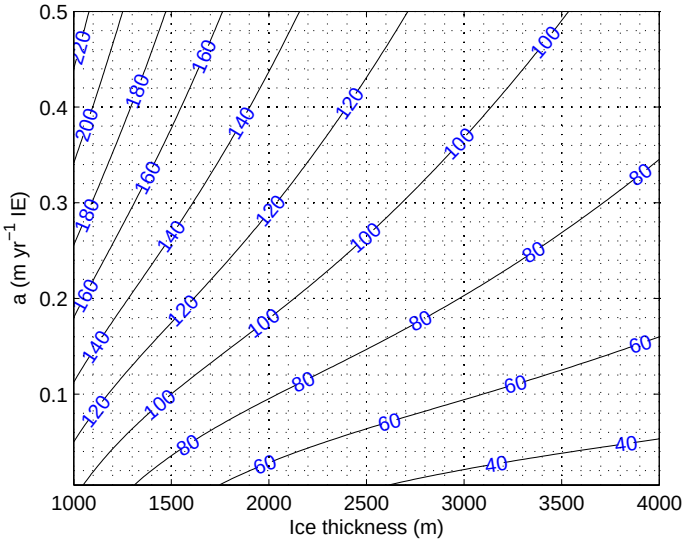

Fig. 1. Minimum GHF (mW m^{-2}) needed to keep the bed at pressure melting point as a function of surface accumulation rate (ice equivalent, IE) and ice thickness and in the absence of horizontal advection. Results are shown for a mean surface temperature of $T_s = -50\,^{\circ}\mathrm{C}$.

CPD
9, 2859–2887, 2013

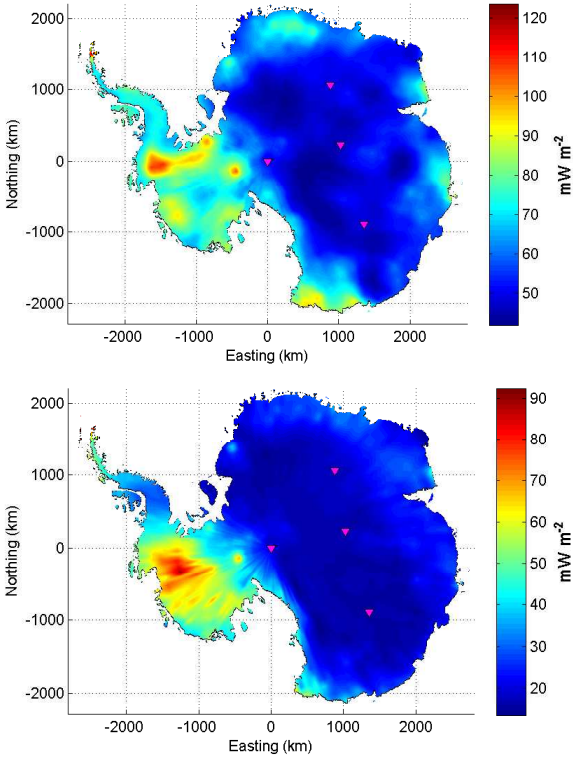

Fig. 2. Top: mean GHF $\overline{G}$ ($\mathrm{mW\,m^{-2}}$) based on GHF estimates by Puruker (2013), Fox-Maule et al. (2005) and Shapiro and Ritzwoller (2004). Bottom: standard deviation σ_G on the GHF datasets. The magenta triangles are the major drill site (from top to bottom): Dome Fuji, Dome Argus, South Pole and Dome Concordia.

CPD
9, 2859–2887, 2013

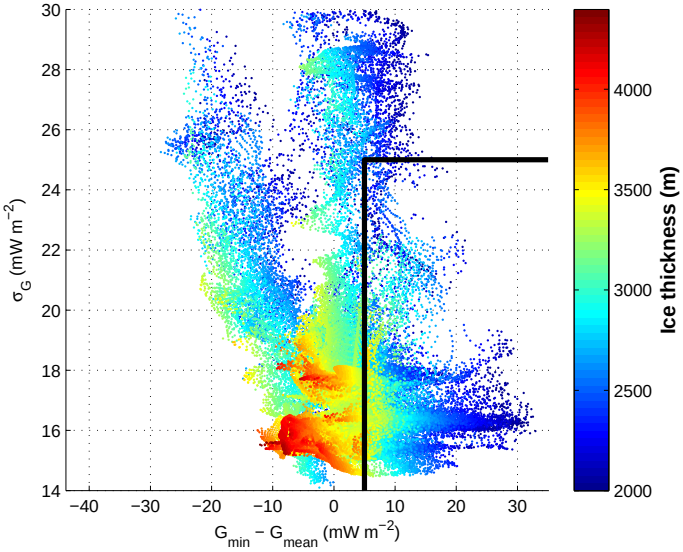

Fig. 3. Scatterplot of $\Delta G = G_{\min} - \overline{G}$ versus σ_G for all points with ice thickness $H > 2000$ m and horizontal flow speed $< 2\,\mathrm{m\,yr^{-1}}$. The colorscale depicts ice thickness for each of the grid points. Negative values of ΔG means that pressure melting point is reached, hence basal melt occurs. Positive values means that the minimum required heat flow to reach pressure melting point is higher than the mean of the three GHF datasets. Points lying within the rectangle are likely to be cold based, taken into account the variability of GHF.

CPD
9, 2859–2887, 2013

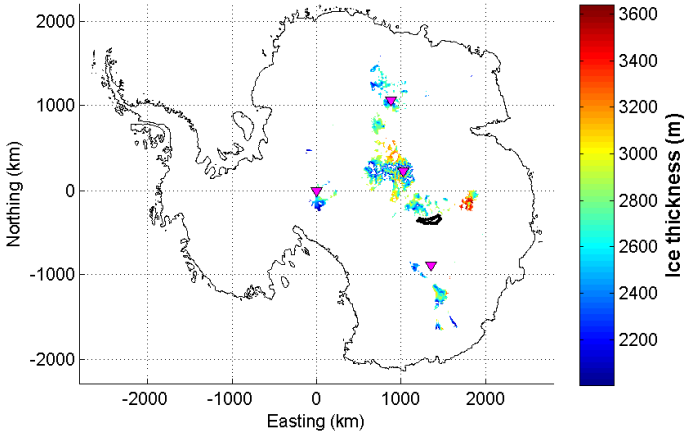

Fig. 4. Potential locations of cold basal conditions in areas with ice thickness $H > 2000\,\mathrm{m}$ (colorbar) and horizontal flow speeds smaller than $2\,\mathrm{m\,yr^{-1}}$, for $\Delta G < 10\,\mathrm{mW\,m^{-2}}$ and $\sigma_G < 10\,\mathrm{mW\,m^{-2}}$, and as calculated with the simple model.

CPD
9, 2859–2887, 2013

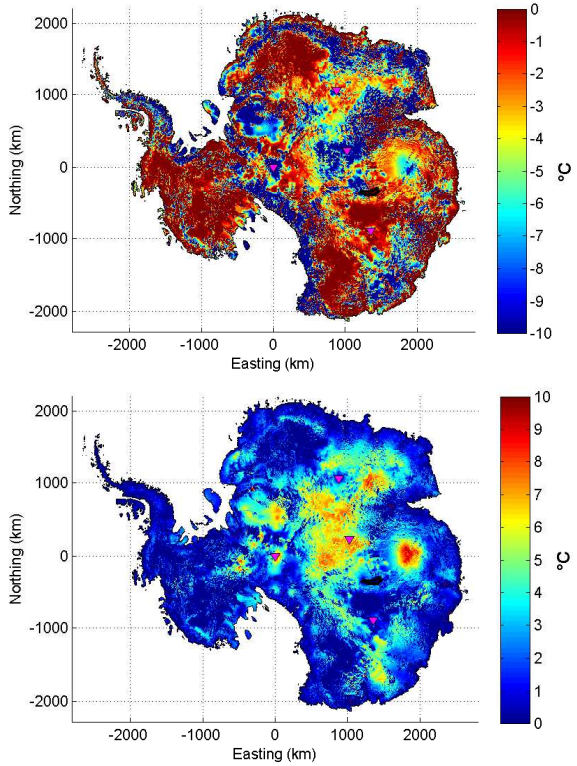

Fig. 5. Top: mean temperature according to the ensemble of 15 experiments (see text for more details), corrected for the dependence on pressure. The lower limit has been cut of at −10 °C. Bottom: Root Mean Square Error (RMSE, °C) according to the same ensemble.

CPD
9, 2859–2887, 2013

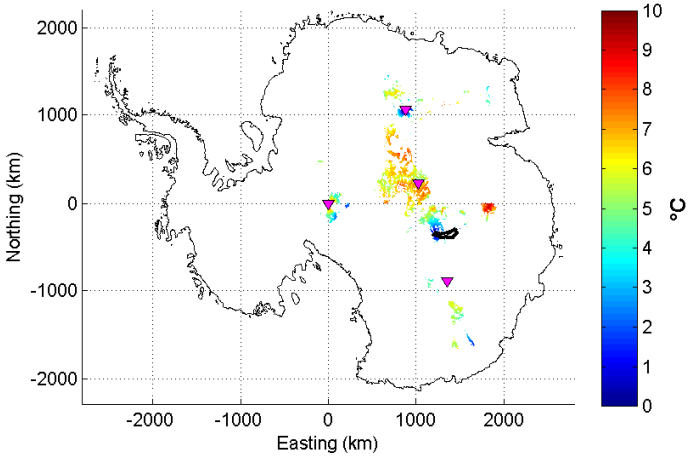

Fig. 6. Potential locations of cold basal conditions in areas with ice thickness $H > 2000$ m, horizontal flow speeds are smaller than $2\,\mathrm{m\,yr^{-1}}$ and basal temperatures as calculated with the full model are lower than $-5\,^{\circ}\mathrm{C}$. The colorbar denotes the RMSE (°C) based on the ensemble calculations.

CPD
9, 2859–2887, 2013

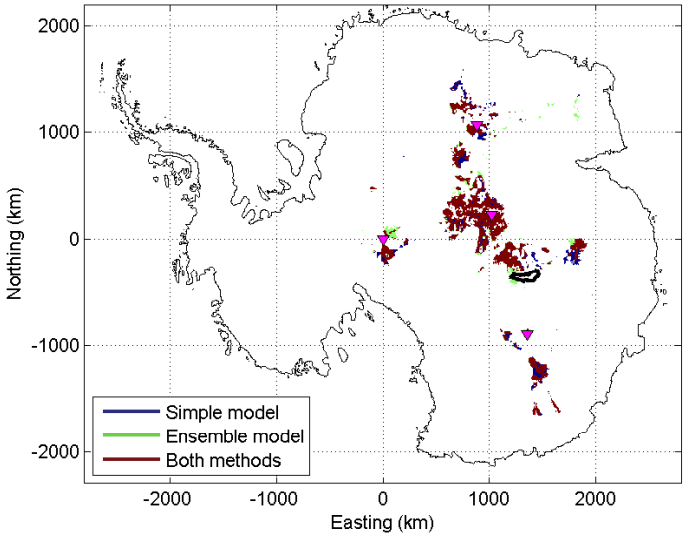

Fig. 7. Potential locations of cold basal conditions in areas with ice thickness $H >$ 2000 m, horizontal flow speeds are smaller than 2 m yr^{-1} according to the simple model (depicted in Fig. 4) and the ensemble model (depicted in Fig. 6).

CPD
9, 2859–2887, 2013